DOI: 10.1021/ma901444u

Macromolecules
ARTICLE

A Quantitative Study of PCBM Diffusion during Annealing of P3HT:PCBM Blend Films

Benjamin Watts,*,†,§ Warwick J. Belcher,‡ Lars Thomsen,‡,⊥ Harald Ade,† and Paul C. Dastoor‡

†*Department of Physics, North Carolina State University, Raleigh, North Carolina 27695, and* ‡*School of Mathematical and Physical Sciences, University of Newcastle, University Drive, Callaghan NSW 2308, Australia.* §*Current address: Paul Scherrer Institut, Villigen 5232, Switzerland.* ⊥*Current address: Australian Synchrotron, Clayton, Victoria 3168, Australia*

Received July 3, 2009; Revised Manuscript Received August 31, 2009

ABSTRACT: Scanning transmission X-ray microscopy has been used to quantitatively map the composition of P3HT:PCBM blend films in the vicinity of PCBM crystals formed during annealing at 140 °C. The observed PCBM concentration profiles around these crystals have been fitted to Fick's second law of diffusion and the diffusion constant found to be 2.5×10^{-14} m^2 s^{-1}. The PCBM concentration at the crystal boundary was found to be 19% (v/v) and is interpreted, together with the annealing temperature of 140 °C, as a point on the bimodal line of the composition−temperature phase diagram. The diffusion of PCBM through P3HT is observed to be bulk-dominated, in contrast to the surface/interface-dominated diffusion observed in MDMO-PPV:PCBM blend films by Yang et al.[1,2]

Introduction

Polymer solar cells are the subject of much research from both academia and industry due to their promise of a cheap, highly scalable renewable source of clean energy. Currently, the most promising polymer solar cell designs are based on bulk heterojunction structures of poly(3-hexylthiophene) (P3HT) and (6,6)-phenyl C_{61} butyric acid methyl ester (PCBM), whereby the electron donor material (P3HT) and the electron acceptor material (PCBM) are blended together in order to optimize both exciton separation and charge transport.[3,4] Postdeposition thermal annealing increases the crystallinity and phase segregation of both the P3HT and PCBM components which improves primarily the hole transport within the film and thus the overall device efficiency.[5−9] These methods were utilized for the current state of the art devices (1:0.9 P3HT:PCBM blend devices annealed at 120 °C), enabling power conversion efficiencies that approach 5%.[5,10−12] However, there appears to be an optimum degree of annealing for maximal efficiency of P3HT:PCBM based devices, with large-scale segregation of the components and large PCBM crystals observed in cases of extended annealing times.[13,14] Bertho et al.[15] have also shown that the long-term stability of such solar cell devices could be limited by further diffusion and aggregation of PCBM during device operation. On the other hand, Li et al.[16] have demonstrated that with careful control over the size and distribution of the PCBM crystals formed during thermal annealing the efficiency of P3HT:PCBM solar cell devices could also be enhanced by the presence of PCBM crystals. The development of polymer solar cells in recent years has largely followed a strategy of optimization; however, for further significant improvements in P3HT:PCBM bulk heterojunction device efficiency and stability to be made, a more sophisticated understanding of the diffusion and aggregation properties of PCBM molecules within the polymer matrix needs to be developed.

*To whom correspondence should be addressed. E-mail: benjamin.watts@psi.ch.

The growth of PCBM crystals in polymer blend films with thermal annealing has been previously studied with techniques such as atomic force microscopy (AFM),[1,13,16−18] transmission electron microscopy (TEM) (and selected area electron diffraction, SAED),[1,2,14−16] scanning near-field optical microscopy (SNOM), and confocal Raman microscopy.[17] These studies have established firm evidence for the presence of a region around each crystal that is depleted of PCBM. Further, they have also shown that the diffusion of PCBM molecules and the growth of PCBM crystals in a polymer matrix can be affected by the annealing temperature and the glass transition temperature (T_g) of the polymer matrix as well as by spatial confinement (by the presence of an impenetrable substrate and/or overlayer). While insightful, these previous studies have been frustrated by their inability to quantify the PCBM concentration. In this work, we utilize scanning transmission soft X-ray microscopy (STXM) to measure quantitatively the depletion of PCBM in the vicinity of large crystals that form during extended annealing of P3HT:PCBM blend films. The nanoscale resolution and molecular structure based contrast mechanism of STXM provides for the calculation of chemical composition maps and thus allows a fully quantitative analysis of the diffusion of PCBM within a polymer matrix. This information will prove valuable in understanding not only the formation of the large crystals that are detrimental to device operation but also the fine-scale segregation that has been shown to aid device efficiency.

Experiment

Regioregular P3HT (MW = 50 000) and PCBM were purchased from Rieke Metals, Inc., and Solenne. P3HT and PCBM were dissolved in chlorobenzene to produce ∼20 g/L concentration solutions with P3HT:PCBM mass ratios of 2:1, 3:2, 1:1, 2:3, and 1:2 (the respective %PCBM vol/vol values of 29.4%, 35.7%, 45.5%, 52.6%, and 62.5% will be referred to from hereon in order to accommodate discussion in terms of Fickian diffusion) and used to produce ∼80 nm films on glass substrates by spin-coating at ∼2000 rpm. These samples were then split into four groups for

 Published on Web 10/07/2009

annealing on a hot plate at 140 °C, which is above the T_g of both P3HT (12.1 °C) and PCBM (131.2 °C),[19] for a range of times both with and without the spatially confining presence of the glass substrate.

The first group of samples, consisting of 45.5% PCBM blend films, was annealed for 10 s, 1 min, 4 min, 40 min, and 12 h. The films were then floated off the glass substrates onto deionized water and onto copper TEM grids for analysis. The second group of samples, also consisting of 45.5% PCBM blend films, was floated onto copper TEM grids before annealing for 10 s, 1 min, 4 min, 40 min, and 12 h. Hence, the first and second sample groups received the same set of treatments, but in a different order such that the annealing was performed with and without spatial confinement by a continuous support surface.

The third sample group consisted of blend films spun from solutions with PCBM concentrations of 29.4%, 35.7%, 52.6%, and 62.5% and were annealed on the hot plate for 4 min. After cooling, the films were floated off the glass substrates onto deionized water and then onto copper TEM grids for analysis (in the same manner as the first group). Note that the 45.5% PCBM blend film annealed for 4 min already exists in the first sample group. The fourth sample group was a control group, consisting of films from each of the blend ratios prepared, floated off onto TEM grids without being subjected to any heat treatment.

The four groups of samples were inspected under an optical microscope in order to both count the density of crystals present in each sample as well as locate appropriate crystal specimens for further observation by STXM.

NEXAFS spectroscopy and X-ray imaging of pristine and blend films were recorded at the 5.3.2 STXM at the Advanced Light Source, Berkeley, CA.[20,21] Figure 1 shows the NEXAFS spectra of the pristine P3HT and PCBM films and demonstrates the photon energy dependent contrast, which is strongest at the photon energies of 285.1 and 288 eV. Representative PCBM crystals identified in the annealed blend films by optical microscope were imaged in the STXM at photon energies providing maximum (285.1 and 288 eV) and minimum (280 and 320 eV) chemical contrast. NEXAFS spectra covering the full carbon K-edge energy region were also measured along a line across each imaged region in order to ensure accuracy of the image data. The sets of images were analyzed to calculate quantitative composition maps of the regions surrounding PCBM crystals, from which concentration profiles perpendicular to the long axis of the crystals were taken for further analysis. Details of the quantitative composition map calculation can be found in a previous communication.[22]

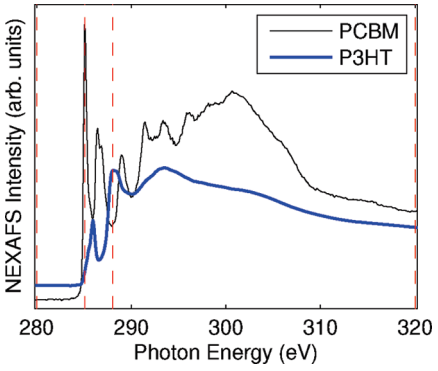

Figure 1. NEXAFS spectra of pristine P3HT and PCBM materials. Vertical, dashed lines indicate the photon energies utilized for imaging blend films.

Results and Discussion

Figure 2 shows optical images of the 45.5% PCBM blend films annealed for 4 min, with the crystals seen as dark, elongated shapes, surrounded by a lighter colored depletion zone. The striped color variations that are especially apparent in the film shown in Figure 2A were found (via STXM) to be caused by small variations in film thickness. Similar optical microscopy revealed that no crystals were present in any of the unannealed films or in any of the films with a PCBM concentration of 29.4% or 35.7%. Crystals were observed in all other films, except for the unconfined 10 s grid-annealed sample. This exception is likely due to the variations in experimental conditions introducing significant error relative to such a short anneal time. Examining Figure 2, a number of common observations are immediately apparent and are summarized in Table 1. First, the crystals grow in size, asymmetry, and number with increasing anneal time. Second, each crystal is surrounded by a depletion region, as has been observed in previous studies of PCBM crystals in polymer matrices.[1,17,18]

It can be seen from Figure 2 and Table 1 that the number density of crystals is much greater in the unconfined grid-annealed films than in the singly confined glass-annealed films. However, a comparison of images A and B in Figure 2 shows that

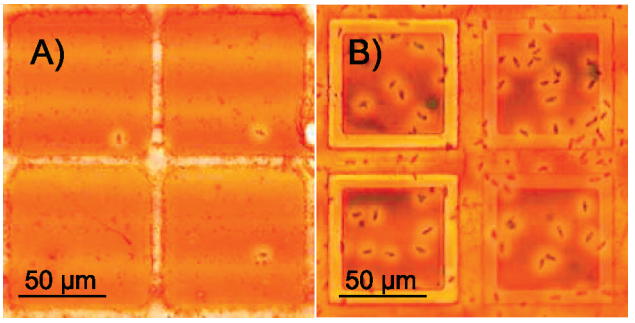

Figure 2. Visible light microscope images of 45.5% PCBM blend films that have been spun onto glass substrates and then (A) annealed for 4 min on the glass substrate before floating onto a TEM grid or (B) floated onto a TEM grid and then annealed for 4 min.

Table 1. Summary of the Observed Number Densities of PCBM Crystals and the Corresponding Average Crystal Separation in Annealed Blend Films with the Composition, Annealing Conditions, and Sample Support Indicated

% PCBM (vol/vol)	anneal time	annealing support	number density of crystals (mm^{-2})	crystal separation (μm)	crystal aspect ratio
45.5	10 s	glass	3.6 ± 2.1	440 ± 230	2.4
45.5	1 min	glass	17 ± 9	250 ± 88	2.0
45.5	4 min	glass	90 ± 17	110 ± 33	2.1
45.5	40 min	glass	99 ± 8	100 ± 37	5.2
45.5	12 h	glass	150 ± 30	81 ± 15	7.5
52.6	4 min	glass	170 ± 56	110 ± 25	7.9
62.5	4 min	glass	530 ± 190	43 ± 3	7.4
45.5	10 s	TEM grid			
45.5	1 min	TEM grid	2600 ± 150	20 ± 2	2.3
45.5	4 min	TEM grid	2700 ± 300	19 ± 1	3.5
45.5	40 min	TEM grid	3400 ± 270	17 ± 1	2.8
45.5	12 h	TEM grid	3500 ± 150	17 ± 1	4.6

despite the difference in the density of crystals formed, the individual crystals and their depletion zones are of similar size and shape. The strong variation in crystal density provides insight into the nucleation of the crystals, suggesting that they nucleate at the film surfaces/interfaces and that the presence of the glass substrate suppresses the nucleation and/or growth of the PCBM crystals. The fact that the crystal density differs by an order of magnitude, rather than a factor of 2, further indicates that the two surfaces/interfaces of the film are not equivalent in terms of crystal nucleation. This observation is supported by previous studies of the vertical structure in spin-cast P3HT:PCBM films, with PCBM tending to be more concentrated at the glass/film interface than at the film/air surface.[23] Thus, the nucleation of PCBM crystals is correlated with the PCBM concentration at the film surface/interface, but the growth of crystals requires unobstructed space to expand. The surface energies of PCBM and P3HT are 38.2 mN/m[24] and 26.9 mN/m,[25] respectively. Consequently, the PCBM concentration is reduced at the film/air surface due to its higher surface energy, and therefore the PCBM concentration and density of crystal nucleation sites is low. However, the film/air surface easily yields space for crystal growth and so these nucleation sites always lead to observed crystals. At the glass/film interface, on the other hand, PCBM is more concentrated, and so there is a high density of nucleation points. However, the presence of the glass substrate frustrates the growth of these crystals, and removal of the film from the glass substrate is required to provide space for these PCBM crystals to grow and the high density of crystals to be observed.

Yang et al.[1,2] studied the effect of spatial confinement on PCBM crystal growth in PCBM:MDMO-PPV films and did not observe the strong difference in crystal nucleation that was observed in these results. Instead, they observed a strong reduction in the aspect ratio of crystals grown in singly confined films, compared to the unconfined films, which they ascribed to frustration of the diffusion of PCBM at the film surfaces/interfaces. However, a suppression of aspect ratio with spatial confinement is not apparent in our experiments (Table 1), and in fact the opposite is observed in the long annealed films; though this observation is more likely due to the higher density of crystals exhausting the supply of PCBM and hence stunting further growth. Thus, the growth of PCBM crystals in P3HT:PCBM blend films is evidently not strongly influenced by spatial confinement during annealing in the same way as that in MDMO-PPV:PCBM blend films. This indicates that the lateral diffusion of small molecules through a P3HT thin film is dominated by bulk diffusion rather than surface or interface effects. Given that P3HT is semicrystalline and that crystallinity impedes diffusion, this seems backward. However, the PCBM diffusion proceeds though the amorphous regions. Given that the T_g of P3HT (12.1 °C[19]) is much lower than that of MDMO-PPV (80 °C[2]), the higher chain mobility and hence increased diffusion related to the T_g seems to be the dominant factor.

Figure 3 shows composition images, calculated from STXM data, in the region of large crystals of the P3HT (left) and PCBM (center) components and the percentage PCBM concentration by volume (right) of 45.5% PCBM blend films that have been annealed on glass substrates (i.e., singly confined) for 10 s (A−C), 1 min (D−F), 4 min (G−I), 40 min (J−L), and 12 h (M−O). The color scale of the component images is quantified in terms of nanometers of material thickness in the scale bars to the right of each image and has been normalized for the average film thickness. Note that the crystals, which are well-known to be pure PCBM and very thick, do not transmit enough photons for a reasonable composition calculation. In addition, higher order spectral contamination and a diffuse halo cause absorption saturation at energies with high absorption in the PCBM. The net effect is that the signal recorded at the location of the crystals

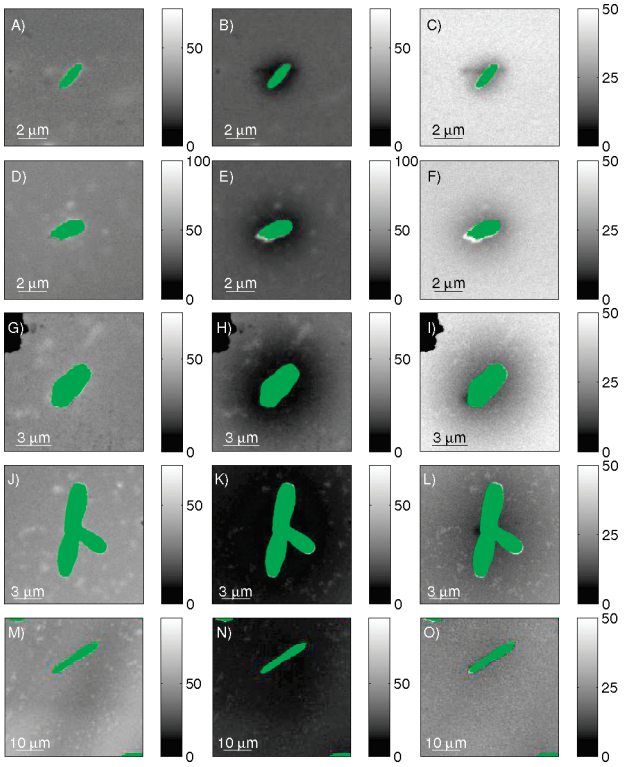

Figure 3. STXM-derived images of the optical density (in terms of component thickness, nm) of P3HT (left), PCBM (center), and the percentage PCBM composition by volume (right) in 45.5% PCBM blend films, in the region of PCBM crystals, annealed for 10 s (A−C), 1 min (D−F), 4 min (G−I), 40 min (J−L), and 12 h (M−O) on a glass substrate. The color scale of the component images has been normalized to the average film thickness. Note that the crystals, which are known to be pure PCBM and very thick, do not transmit enough photons for a reasonable composition calculation. Pixels with a χ value greater than 0.1 returned by the spectral fitting function have been colored green to indicate an absence of reliable composition information.

is higher than it should be. This is reflected in the χ values returned by the spectral fitting routine, and hence the pixels in Figure 3 at which the χ value is greater than 0.1 have been colored green to indicate an absence of reliable composition information. These experimental artifacts do not significantly affect the measurements and composition calculations at positions outside of the crystal.

Interestingly, the PCBM images in Figure 3 show a dark region surrounding the crystals. These dark regions signify a depletion of PCBM in the vicinity of the PCBM crystals and grow with anneal time at a greater rate than the crystals themselves. In contrast, the P3HT images on the left of Figure 3 show that no lateral migration of the polymer material occurs in the regions outside the PCBM crystals. It seems reasonable to hypothesize that the PCBM depletion near the PCBM crystals is due to the diffusion of the PCBM molecules into the growing PCBM crystals, which create a localized sink as previously discussed by Klimov et al.[17] and Zhong et al.[18] Thus, it would appear that the P3HT polymer is acting as a matrix in which PCBM molecules have significant mobility at the annealing temperature of 140 °C. Moreover, using AFM, Zhong et al.[18] observed a decrease in the film thickness in the region around the PCBM crystals that mirrors the PCBM concentration observed in Figure 3. These observations indicate that the P3HT has sufficient mobility to collapse any voids left by the reduced volume of PCBM. The STXM images of crystals from other films were found to share identical features and trends as those shown in Figure 3 and are presented in the Supporting Information.

The generation of quantitative composition maps from STXM data enables a more sophisticated investigation of PCBM diffusion, which should obey Fick's second law of diffusion:[26]

$$\frac{\partial \phi}{\partial t} = -D\frac{\partial^2 \phi}{\partial^2 x}$$

where ϕ represents the PCBM concentration (in terms of volume) and D represents the diffusion constant, while x and t represent dimensions of space and time. Fick's second law of diffusion simply states that the rate of movement of a diffusing species is negatively proportional to the curvature of its concentration gradient. The constant of proportionality is the diffusion constant of the species in that medium (and at that temperature).

While Campoy-Quiles et al.[23] observed vertical composition gradients and layered structures within P3HT:PCBM films, the PCBM depletion region observed here extends laterally over ~10 μm, which is 2 orders of magnitude greater than the film thickness of ~100 nm, and so we can safely ignore the film thickness in the analysis of the observed PCBM diffusion toward the crystal. We further reduced the system to a one-dimensional model by taking advantage of the high aspect ratio of the crystals and considering the PCBM composition profile perpendicular to the long axis of the crystal. These one-dimensional PCBM diffusion profiles were then compared to calculated profiles from the following solution to Fick's law:[27]

$$\phi = \phi_b + (\phi_0 - \phi_b)\frac{4}{\pi}\sum_{m=1}^{\infty}\frac{1}{m}\sin\left(\frac{m\pi x}{L}\right)\exp\left(-Dt\left(\frac{m\pi}{L}\right)^2\right)$$

where ϕ_0 and ϕ_b represent the initial PCBM concentration within the film and the equilibrium PCBM concentration at the crystal wall, respectively. L represents the distance between neighboring crystals, t represents time, and D represents the diffusion constant. Figures 4, 5, and 6 show the experimentally observed PCBM profiles (points) and the fitted set of Fick diffusion profiles (lines), all calculated with the same values for the diffusion constant and equilibrium PCBM concentration.

The boundary values, ϕ_b, for the Fick solution were set to a constant PCBM concentration value, which can be interpreted as the concentration at which the rate of incorporating new PCBM molecules into the crystal is balanced by the osmotic back-diffusion and would represent the position of the coexistence line in a composition−temperature phase diagram. The initial PCBM concentration, ϕ_0, and anneal time were entered into the calculation from the preparation parameters of each sample film. The spatial range over which the solution was calculated was set to the calculated average crystal separation for the 12 h annealed samples from Table 1. The same crystal separation distance was used for each set of samples, despite the fact that Table 1 clearly shows a trend in crystal density with anneal time, because only the longest annealed samples displayed large enough depletion zones for their diffusion profiles to be affected by neighboring crystals. In other words, the crystal separation distance is irrelevant for any sample for which it is not set to a realistic value in the diffusion profile calculation. The inset of Figure 4, where the solutions are plotted over the full range of the calculation, illustrates this effect with only the 12 h profile exhausting the supply of virgin film between the modeled crystals for the singly confined set. Similarly, this strategy of using only the minimum crystal separation for the calculation of PCBM profiles is also successful for the unconfined sample set, as shown in Figure 6, and is moot for the varying concentration series shown in Figure 5 due to the short anneal time and correspondingly short reach of the observed depletion zones.

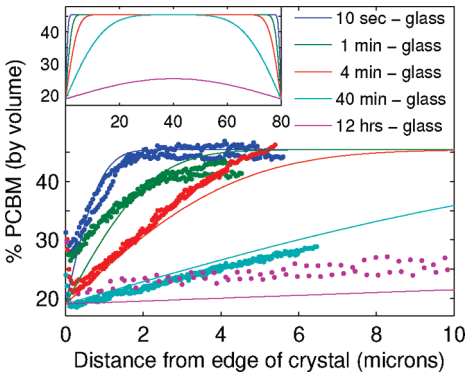

Figure 4. Comparison of a time series of experimental (points) and modeled (lines) PCBM concentration profiles of glass-annealed 45.5% PCBM blend films. The inset shows the full spatial extent of the model.

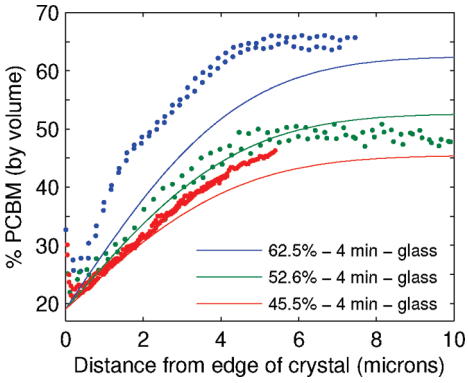

Figure 5. Comparison of a concentration series of experimental (points) and modeled (lines) PCBM concentration profiles of 4 min glass-annealed P3HT:PCBM blend films with initial blend ratios (PCBM concentrations) of 45.5%, 52.6%, and 62.5%.

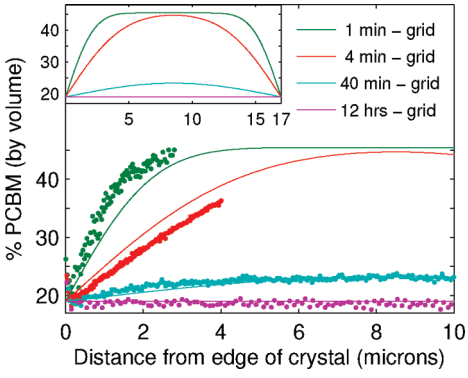

Figure 6. Comparison of a time series of experimental (points) and modeled (lines) PCBM concentration profiles of TEM grid-annealed 45.5% PCBM blend films. The inset shows the full spatial extent of the model. As stated in the text, no crystals were observed in the unconfined 10 s grid-annealed blend film, and as such this series has been omitted from this figure.

A weakness of the diffusion model used here is that the boundary of the crystal is assumed to be fixed, which is obviously not true since the crystal grows laterally with time. Taking this effect into account would greatly complicate the boundary condition of the partial differential equation. However, since the crystals grow in height (vertical thickness) and length at a far greater rate than in width, the effect of the moving crystal boundaries is not expected to have a significant impact on the PCBM concentration profiles discussed here, since they have

been measured perpendicular to the long axis of the crystal where the rate of expansion of the crystal is least.

As shown in Figures 4, 5, and 6, the model was found to best fit the set of experimental profiles with a diffusion constant of 2.5×10^{-14} m^2 s^{-1} and an equilibrium PCBM concentration of 19%. Note that the calculated Fick solutions shown in Figures 4, 5, and 6 have all used the same values for the diffusion constant and equilibrium PCBM concentration. The appropriateness of these values can be seen from the shape of the calculated curve and its comparison to the experimental data. The diffusion constant appears in the equation of the Fick solution above as a coefficient for the time variable and therefore modulates the progress of the diffusion process with time and can be discussed in terms of the position of the knee of the profile. The position of the knee of the plotted Fick solution profiles can be seen to fit the experimental diffusion profiles without any systematic error that would indicate evidence for variation of the diffusion constant. Therefore, we can see that the diffusion constant of PCBM within a P3HT matrix is identical in both unconfined (grid-annealed) and singly confined (glass-annealed) films and so is not significantly affected by surface/interface effects, which further supports our earlier argument that the diffusion of PCBM within a P3HT matrix is dominated by the bulk. On the other hand, there are some random variations in the position of the knee of the calculated profiles compared to the corresponding experimental diffusion profiles. This is most apparent in the 1 and 4 min grid-annealed profiles in Figure 6; however, such random error is more easily attributed to errors in time than variations in the diffusion constant, especially since the grid supported films are more difficult to handle and so are more likely to experience increased timing errors in their preparation.

Before discussing the appropriateness of the fitted value of the equilibrium PCBM concentration, let us first discuss the meaning and implications of this term. One could infer from the obtained equilibrium PCBM concentration, ϕ_b, that the limiting PCBM concentration at which crystals can form and grow is 19%. However, in these experiments, sample films were prepared with PCBM concentrations of 29.4% and 35.7% in which no crystals were observed after annealing. Linearly extrapolating the crystal densities listed in Table 1 toward zero at a PCBM concentration of 19% allows us to calculate that approximately 25 and 60 crystals per square millimeter of film ought to have been present in the 29.4% and 35.7% sample films respectively, which would have been easily observable. Therefore, simply interpreting the PCBM equilibrium concentration in such a way is clearly inconsistent. A better interpretation is found by discussing the situation in terms of a composition−temperature phase diagram, in which a composition of 19% at 140 °C would correspond to a point on the coexistence or bimodal curve. PCBM concentrations of 29.4% and 35.7% would most likely reside in the nucleation and growth region with a metastable condition. For 45.5% PCBM blends, which are deeper in the two phase region, it becomes easier to encounter critical fluctuations that can nucleate a crystal. We note that the 45.5% composition might be close the spinodal line that delineates the spontaneous unstable region in the phase diagram. TEM images of 45.5% blends are very reminiscent of the bicontinuous morphology that one would expect for spinodal decomposition.[5]

Now, the appropriateness of the 19% value utilized for the equilibrium PCBM concentration in the calculated Fick solution profiles can be seen in the PCBM concentration adjacent to the crystal wall in Figures 4, 5, and 6. Interestingly, while Figure 4 shows strong variation in the experimentally observed PCBM concentration adjacent to the crystal wall, Figure 6 shows no such variation. The difference can be understood from the nature of the substrates and their impact on experimental conditions. The samples shown in Figure 4 were annealed on glass, which is much less thermally conducting than the copper TEM grids on which the samples shown in Figure 6 were annealed on. This resulted in greater experimental error in annealing temperature for the glass-annealed samples, with the sample film likely to have been typically lower than intended. At lower temperature, the trajectory of an annealing sample across the phase diagram would intersect the bimodal curve at a different composition value, resulting in a different PCBM equilibrium temperature being observed. The observation that higher equilibrium PCBM concentrations were seen in the glass-annealed films which presumably experienced lower annealing temperatures suggests that the bimodal curve has a negative and not very steep gradient near the point (19%, 140 °C) in the composition−temperature phase diagram. This observation further suggests that future experiments could utilize the diffusion profiles around PCBM crystals in P3HT:PCBM films annealed at a range of precisely known temperatures to experimentally map out the bimodal curve of the P3HT:PCBM phase diagram.

Conclusions

A thorough understanding of the diffusion of PCBM within a polymer matrix is essential to the production of film nanostructures that provide high-efficiency polymer devices as well as to the longevity of such devices. In this work, we have quantitatively mapped the composition of annealed P3HT:PCBM thin films in the region around large PCBM crystals and compared the observed PCBM profiles to calculated solutions to Fick's second law of diffusion to determine the diffusion constant and equilibrium concentration of PCBM within a P3HT matrix at 140 °C to be 2.5×10^{-14} m^2 s^{-1} and 19%, respectively. The equilibrium PCBM concentration of 19% at 140 °C is interpreted as a point on the bimodal curve of the composition−temperature phase diagram. We further hypothesize that PCBM concentrations of 29.4% and 35.7%, in which samples no crystals were observed, are metastable and that 45.5% is deeper in the two-phase region of the phase diagram, possibly close to the spinodal line that delineates the spontaneous unstable region in the phase diagram. The number of observed PCBM crystals in annealed P3HT:PCBM blend films increases dramatically when the films are floated onto grids before annealing. This effect is attributed to a combination of vertical segregation of the spin-cast blend film,[23] concentrating the PCBM close to the glass substrate and spatial confinement, where the presence of the glass substrate suppresses the growth of the crystals nucleated at the interface. We observe that while the nucleation and growth of PCBM crystals is hindered by the spatial confinement of a solid substrate, the diffusion of PCBM molecules within a P3HT matrix is not affected by spatial confinement. We therefore conclude that the low T_g of P3HT allows diffusion to proceed through the polymer bulk in contrast to the higher T_g polymer, MDMO-PPV, the PCBM diffusion through which was observed by Yang et al.[1,2] to be limited to the surfaces/interfaces and thus heavily affected by spatial confinement.

Acknowledgment. The ALS is supported by the Director of the Office of Science, Department of Energy, under Contract DE-AC02-05CH11231. Work at NCSU (B.W. and H.A.) was supported by US Department of Energy under Contract DE-FG02-98ER45737. This work was supported by the Australian Research Council's Discovery funding scheme (DP0559417).

Supporting Information Available: STXM-derived images of the entire experimental set of PCBM crystals in annealed P3HT:PCBM blend films. This material is available free of charge via the Internet at http://pubs.acs.org.

References and Notes

(1) Yang, X.; Alexeev, A.; Michels, M. A. J.; Loos, J. *Macromolecules* **2005**, *38*, 4289–4295.
(2) Yang, X.; van Duren, J. K. J.; Janssen, R. A. J.; Michels, M. A. J.; Loos, J. *Macromolecules* **2004**, *37*, 2151–2158.
(3) Halls, J. J. M.; Walsh, C. A.; Greenham, N. C.; Marseglia, E. A.; Friend, R. H.; Moratti, S. C.; Holmes, A. B. *Nature* **1995**, *376*, 498–500.
(4) Yu, G.; Gao, J.; Hummelen, J. C.; Wudl, F.; Heeger, A. J. *Science* **1995**, *270*, 1789–1791.
(5) Ma, W. L.; Yang, C. Y.; Gong, X.; Lee, K.; Heeger, A. J. *Adv. Mater*. **2005**, *15*, 1617–1622.
(6) Kim, K.; Liu, J.; Namboothiry, M. A. G.; Carroll, D. L. *Appl. Phys. Lett*. **2007**, *90*, 163511.
(7) Vanlaeke, P.; Swinnen, A.; Haeldermans, I.; Vanhoyland, G.; Aernouts, T.; Cheyns, D.; Deibel, C.; D'Haen, J.; Heremans, P.; Poortmans, J.; Manca, J. V. *Sol. Energy Mater. Sol. Cells* **2006**, *90*, 2150–2158.
(8) Zhokhavets, V.; Erb, T.; Hoppe, H.; Gobsch, G.; Sariciftci, N. S. *Thin Solid Films* **2006**, *496*, 679–682.
(9) Yang, X.; Loos, J.; Veenstra, S. C.; Verhees, W. J. H.; Wienk, M. M.; Kroon, J. M.; Michels, A. J.; Janssen, R. A. J. *Nano Lett*. **2005**, *5*, 579–583.
(10) Green, M. A.; Emery, K.; Hishikawa, Y.; Warta, W. *Prog. Photovolt*. **2008**, *16*, 61–67.
(11) Dennler, G.; Scharber, M. C.; Brabec, C. J. *Adv. Mater*. **2009**, *21*, 1–16.
(12) Reyes-Reyes, M.; Kim, K.; Carroll, D. L. *Appl. Phys. Lett*. **2005**, *87*, 083506.
(13) Chirvas, D.; Paris, J.; Hummelen, J. C.; Dyakonov, V. *Nanotechnology* **2004**, *15*, 1317–1323.
(14) Savenije, T. J.; Kroeze, J. E.; Yang, X.; Loos, J. *Adv. Funct. Mater*. **2005**, *15*, 1260–1266.
(15) Bertho, S.; Janssen, G.; Cleij, T. J.; Conings, B.; Moons, W.; Gadisa, A.; D'Haen, J.; Goovaerts, E.; Lutsen, L.; Manca, J.; Vanderzande, D. *Sol. Energy Mater. Sol. Cells* **2008**, *92*, 753–760.
(16) Li, L.; Lu, G.; Li, S.; Tang, H.; Yang, X. *J. Phys. Chem. B* **2008**, *112*, 15651–15658.
(17) Klimov, E.; Li, W.; Yang, X.; Hoffmann, G. G.; Loos, J. *Macromolecules* **2006**, *39*, 4493–4496.
(18) Zhong, H.; Yang, X.; deWith, B.; Loos, J. *Macromolecules* **2006**, *39*, 218–223.
(19) Zhao, J.; Swinnen, A.; Van Assche, G.; Manca, J.; Vanderzande, D.; Van Mele, B. *J. Phys. Chem. B* **2009**, *113*, 1587–1591.
(20) Kilcoyne, A. L. D.; Tyliszczak, T.; Steele, W. F.; Fakra, S.; Hitchcock, P.; Franck, K.; Anderson, E.; Harteneck, B.; Rightor, E. G.; Mitchell, G. E.; Hitchcock, A. P.; Yang, L.; Warwick, T.; Ade, H. *J. Synchrotron Radiat*. **2003**, *10*, 125–136.
(21) Warwick, T.; Ade, H.; Kilcoyne, A. L. D.; Kritscher, M.; Tylisczcak, T.; Fakra, S.; Hitchcock, A. P.; Hitchcock, P.; Padmore, H. A. *J. Synchrotron Radiat*. **2002**, *9*, 254–257.
(22) McNeill, C. R.; Watts, B.; Thomsen, L.; Belcher, W J.; Greenham, N. C.; Dastoor, P. C. *Nano Lett*. **2006**, *6*, 1202–1206.
(23) Campoy-Quiles, M.; Ferenczi, T.; Agostinelli, T.; Etchegoin, P. G.; Kim, Y.; Anthopoulos, T. D.; Stavrinou, P. N.; Bradley, D. D. C.; Nelson, J. *Nat. Mater*. **2008**, *7*, 158–164.
(24) Björström, C. M.; Nilsson, S.; Bernasik, A.; Budkowski, A.; Andersson, M.; Magnusson, K. O.; Moons, E. *Appl. Surf. Sci*. **2007**, *253*, 3906–3912.
(25) Wang, X.; Ederth, T.; Inganäs, O. *Langmuir* **2006**, *22*, 9287–9294.
(26) Fick, A. *Ann. Phys. Chem*. **1855**, *94*, 59–86.
(27) Tuck, B. *Introduction to Diffusion in Semiconductors*; Peregrinus: Salisbury, 1974.